N93-29645

# PROGRESS REPORT ON THE HEAVY IONS IN SPACE (HIIS) EXPERIMENT

James H. Adams, Jr., Lorraine P. Beahm, Paul R. Boberg,[1*] and Allan J. Tylka
E. O. Hulburt Center for Space Research
Code 7654, Naval Research Laboratory
Washington, DC 20375-5352
Phone: 202/767-2747, Fax: 202/767-6473

## SUMMARY

One of the objectives of the Heavy Ions In Space (HIIS) experiment is to investigate heavy ions which appear at LDEF below the geomagnetic cutoff for fully-ionized galactic cosmic rays. Possible sources of such "below-cutoff" particles are partially-ionized solar energetic particles, the anomalous component of cosmic rays, and magnetospherically-trapped particles. In recent years, there have also been reports of below-cutoff ions which do not appear to be from any known source[1-5]. Although most of these observations are based on only a handful of ions, they have led to speculation about "partially-ionized galactic cosmic rays" and "near-by cosmic ray sources"[4-6]. The collecting power of HIIS is orders of magnitude larger than that of the instruments which reported these results, so HIIS should be able to confirm these observations and perhaps discover the source of these particles. We report here preliminary results on below-cutoff heavy-ions. We compare our observations to possible known sources of such ions.

A second objective of the HIIS experiment is to measure the elemental composition of ultraheavy galactic cosmic rays, beginning in the tin-barium region of the periodic table. We also briefly report on the status of this analysis.

## THE HIIS DETECTOR SYSTEM

The HIIS detectors were contained in two trays (H3 and H12) on the space-facing end of LDEF. Each tray contained four modules. Fig. 1 shows one of the HIIS trays and a cut-away of one of the modules. Each module comprised two separate stacks of plastic track detectors, a main stack which was sealed in one atmosphere of dry air and a top stack which was in vacuum. The main stack was constructed primarily of 10-mil thick sheets of CR-39[7], which were cast by Pershore Mouldings Ltd. (Pershore, UK) according to a special process for producing highly-uniform, detector-quality material which we developed[8]. The CR-39 sheets were cast from resin containing 1% dioctylphthalate[9]. The main stack also contained a few 5- and 10-mil thick sheets of Lexan[10]. The Lexan we used was manufactured especially for us without UV stabilizer, so as to make it possible to enhance the latent tracks with ultraviolet light[11]. The top stack consisted of 25 5-mil Lexan sheets. The total vertical thickness of the detector module was ~12 g/cm$^2$. The total number of detector sheets is 2782, each of which has an area of 1064 cm$^2$. Total collecting power of the eight detector modules is $A\Omega = 2.0$ m$^2$-sr. HIIS is one of the largest cosmic ray detectors ever flown in space, second only to the Ultra Heavy Cosmic Ray Experiment (UHCRE)[12], which also flew on LDEF.

Seven of our eight modules were constructed as described above. The eighth module was of a special design so as to extend the detector's range to lower energies. In this module both stacks were sealed in an atmosphere of dry air and the honeycomb lid shown Fig. 1 was replaced with four thin Kapton[13] windows.

---

[1*] NRC Postdoctoral Research Associate

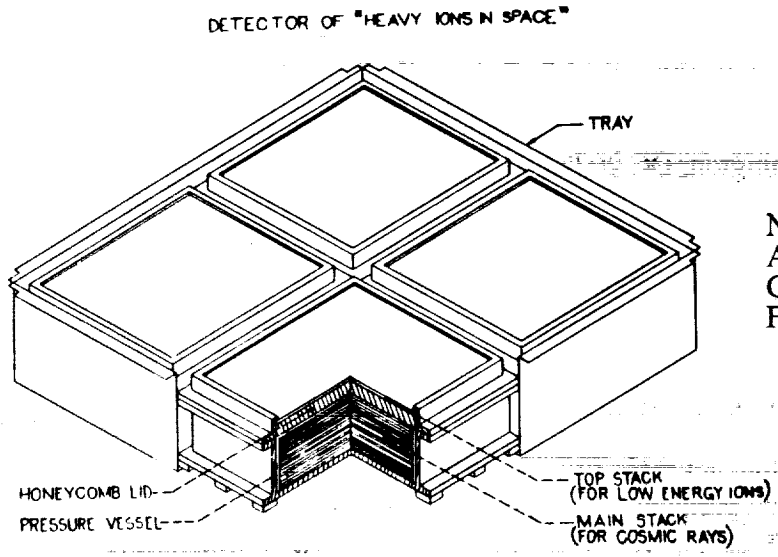


TABLE 1 Stopping Ion Energies (MeV/n)

| | Top Stack | Main Stack |
|---|---|---|
| Ne | 18 - 57 | 72 - 334 |
| Ar | 23 - 89 | 87 - 767 |
| Ca | 26 - 100 | 106 - 887 |
| Fe | 27 - 111 | 117 -1022 |

Figure 1: One of the two LDEF trays containing the HIIS experiment. Each tray contained four modules, one of which is shown in a cut-away here. Table 1 at the right shows the energy range for various stopping ions in the top and main detector stacks.

## METHOD OF DETECTION

Plastic track detectors record charged particles by the trails of radiation damage they leave as they pass through the detector sheets. These tracks, which are revealed by chemically etching the detectors, are a permanent record of the particle's path and its rate of ionization in the plastic. The response of a plastic track detector is characterized by $V_T/V_B$, where $V_T$ is the rate at which plastic is etched away along the damage trail and $V_B$ is the rate at which bulk undamaged plastic is dissolved by the etchant. Because of radiation damage to the polymer, $V_T/V_B > 1$. The competition between $V_T$ and $V_B$ leads to the formation of a conically shaped etch pit whenever

$$(V_T/V_B)\cos(\theta) > 1 \qquad (1)$$

where $\theta$ is the angle between the trajectory of the charged particle and the normal to the detector sheet[14]. $V_T/V_B$ is empirically found to be an increasing function of the restricted energy loss[15] (REL), which provides a numerical measure of the radiation damage generally dependent upon atomic number Z, mass number A, and the particle velocity $\beta$. Etch pits are measured under a high precision microscope. From the displacement of etch pits on the bottom and top surfaces of a detector sheet, the incidence angle $\theta$ can be measured. $V_T/V_B$ can be determined by measuring the dimensions of the etch pit[16,17].

Stopping ions are identified by following them to where they came to rest in the detector and by measuring $V_T/V_B$ in each detector surface along the particle's trajectory. When these $V_T/V_B$ values are plotted versus the distance to the end of the track (the so-called "residual range"), they fall upon characteristic curves determined by Z and (weakly) by A. Once the particle's identity is known, its total range in the detector specifies its incident energy.

For relativistic particles, REL (and hence $V_T/V_B$) is nearly constant as the particle traverses the detector. $V_T/V_B$ can be precisely determined by averaging measurements from many detector surfaces. $V_T/V_B$ depends primarily upon the atomic number Z and only very weakly upon the particle velocity $\beta$, so the average $V_T/V_B$ value identifies Z even without a measurement of $\beta$.

## POST-FLIGHT ASSESSMENT OF THE DETECTOR PERFORMANCE

In the Proceedings of the First LDEF Post-Retrieval Symposium, we published a detailed report on the post-flight condition of the detectors[18]. In this section we briefly summarize those results. The reader is referred to those Proceedings for more detailed information.

*Temperature Effects.* The single most important factor affecting the performance of track detectors is temperature. In particular, good elemental resolution requires that the temperature of the detector stack be maintained within narrow limits. In HIIS this was accomplished by a carefully-designed passive thermal control system. A detailed post-flight thermal analysis indicated that this system would hold the temperature of the main detector stacks in the range of -7.5 $\pm$ 2.0 °C, a somewhat better performance than predicted in pre-flight analysis.

At some point in the mission, part of the HIIS thermal control system failed: the thermal blankets protecting the HIIS modules partially detached and rolled up, exposing parts of the top detector stacks to solar UV. The pattern of UV and atomic oxygen damage on the surfaces of the blankets suggests that the failure occurred in the last few months of the mission, during which LDEF was at lower altitudes and vulnerable to atomic oxygen damage. The degree of blanket failure varied from module to module. Post-flight examination of the blankets revealed that the failures were due to shrinkage of the top face sheets, perhaps because of the loss of some reactive or volatile component, causing them to tear loose from the modules. Post-flight thermal analysis indicates that without the blankets, the main stacks were colder (average temperature -13.0 °C) and underwent a larger range of temperature (rms width 2.3 °C).

Even with the partial failure of the thermal blankets, it appears that temperature variation had negligible effect on HIIS elemental resolution, at least in the main detector stacks. Although the post-flight examination of the blankets suggests that they failed near the end of the mission, we do not know this for certain. We therefore took a conservative approach in simulating temperature effects on the detectors: we assumed the "worst case" scenario, in which the blankets failed half-way through the mission, thereby producing the widest possible range of temperature variation. We folded this thermal history with results from accelerator studies of temperature effects for particles with comparable $V_T/V_B$ values. Even in this worst case, we find that temperature effects are small: for stopping Fe tracks, the charge peak is broadened by less than 0.05 charge unit. The width of the relativistic Z=60 charge peak increases by less than 0.1 charge unit. For more heavily-ionizing particles, temperature smearing is more severe. In all cases, temperature effects appear to have a minor effect on the elemental resolution.

*Post-Flight Condition of the Detectors.* The HIIS main detector stacks were originally sealed in 1 atm of dry air. The special module with the Kapton windows leaked because the windows were punctured by micrometeoroids after the thermal blanket rolled up. We analyzed the air in the remaining modules and compared it with air from the bottle used to fill the modules before flight. This air contained 10% helium as a tracer. The same helium concentration was found in the post-flight modules, proving that they did not leak. The analysis of the gas in the modules did, however, reveal a change in composition. The concentration of $O_2$ varied from module to module, with values in the range of 12-20% of the pre-flight concentration. Most of the $O_2$ had been replaced by $CO_2$, but some was no longer in gaseous form. Since the detector sheets almost completely filled the module volume, residual oxidation and polymerization of the CR-39 after the modules were sealed can easily account for the missing oxygen. CR-39 is known to oxidize in room air. Also, oxygen is consumed during the polymerization process. The HIIS CR-39 was manufactured over a six month period, and some sheets were freshly polymerized when the modules were sealed. This could account for the variation among modules in the residual $O_2$ concentration. If residual polymerization is the explanation of the missing $O_2$, the oxygen concentrations probably leveled out to near their final value prior to launch.

After analyzing the gas in the detector modules, the main detector stacks were disassembled. The detector sheets in the main stacks were not damaged, discolored, or stuck together. To date we have etched 50 sheets from the main stacks in two detector modules: module C, in which the residual $O_2$ concentration was lowest; and module E, in which the residual $O_2$ concentration was highest. (Oxygen plays a role in fixing the radiation damage in CR-39[19].) These two modules also showed different degrees

of thermal blanket failure. In Module C, the thermal blanket was nearly intact, with only a tear in the few topmost layers. Module E had one of the most severely damaged blankets. By choosing these two modules, we believe that our initial examination brackets the range of sensitivities in the HIIS detectors.

In all of the etched sheets, we found both relativistic and stopping cosmic ray tracks. These tracks were easily found by either manual or automated scanning. None of the sheets was overexposed, and surface features did not interfere with measurements of the cosmic ray tracks. On the basis of our measurement and analysis of these tracks, we conclude that the main detector stacks, at least in the seven modules which did not leak, contain valuable cosmic ray data.

With regard to the top detector stacks, six of the seven were partially exposed to the sun. The seventh stack remained protected by a thermal blanket. It appears to be in excellent condition and should be useable for measuring fluxes of low energy particles (see Fig. 1). It is also possible that the protected portions of the other top stacks may be useable as well, since they show no sign of UV exposure.

## CALIBRATION OF THE HIIS DETECTORS

We conducted extensive pre-flight Bevalac calibrations of the HIIS detectors. Our present plan, however, is to internally calibrate the detectors, using the cosmic rays themselves. The detector sheets we have etched so far contained tracks, but not in the numbers we expected. Relativistic Fe, for example, appears not to have been recorded[2*] . The density of shallow surface pits (due to trapped protons) was also much less than expected. Such apparent reduction in CR-39's sensitivity has been observed before[20]; it is consistent with the reduced oxygen concentration in the modules[19].[3*]

Because the observed detector response is so different from that in accelerator exposures, we believe that "boot-strapping" from the observed cosmic ray tracks is the most reliable calibration method. This method also ensures that the environmental effects on the HIIS detectors, whatever they may have been, will be reflected in the detector calibration. Also, since the residual oxygen concentration varied from module to module, a separate calibration must be derived for each module.

Because we did not wish to risk losing valuable cosmic ray data to overetching, we began our analysis by etching sheets near the bottoms of Modules C & E, at a vertical depth of ~11 g/cm$^2$ in the detector. In each module, we found a sample of ~40 long stopping tracks with precisely measured stopping ends. We have used these tracks to calibrate the modules: our thermal modeling indicates that the temperature in the main detector stacks should have been uniform to within 0.3°C, so the calibration should be the same throughout.

To illustrate this internal calibration method, Fig. 2 shows the raw data from stopping tracks in CR-39 near the bottom of Module E. The data organize themselves into densely populated bands, with no tracks above the topmost band. This indicates a sudden drop in the elemental abundance of the ions. According

---

[2*] This absence of relativistic Fe tracks confirms that the HIIS detectors did not go into space with their full sensitivity. On the basis of pre-flight calibrations in 1 atm of air, we expected the HIIS detectors to record 2500/cm$^2$ relativistic Fe tracks. A detailed manual scan of ~100 cm$^2$ found no relativistic Fe tracks. We know of no mechanism for the fading of such tracks, since CR-39 detectors on other LDEF experiments and detectors stored on the ground in comparable temperature conditions show no such effect over six years. The absence of recorded relativistic Fe tracks thus indicates that the HIIS detectors could not have been in space at the their normal sensitivity for more than an hour!

[3*] Portions of some detector sheets had been exposed to a stopping Fe beam at the Bevalac before they were sealed in the HIIS modules for flight. After retrieval, we removed these sheets from the modules and exposed them again to the same beam, in 1 atm of air. $V_T/V_B$ measurements in the two sets of tracks are identical to within measurement errors, further confirming that the suppressed detector sensitivity was due to the reduced oxygen concentration in the modules. The comparison between the two sets of tracks also indicates that no significant amount of thermal annealing occurred during the flight.

to the general abundance of elements, there are only two places in the periodic table where such a drop occurs, above Fe and above Pb. Pb ions are far too rare to explain the observed fluxes, so we identified the tracks in the topmost band as Fe. The most-lightly ionizing track in the dataset was identified as S by demanding that its calculated ionization rate at small residual range be consistent with that of the Fe tracks at large residual range. The Fe and S tracks were used to fit the detector response function shown in Fig. 3. (The calibration of Module C was similar. See Ref. 21.)

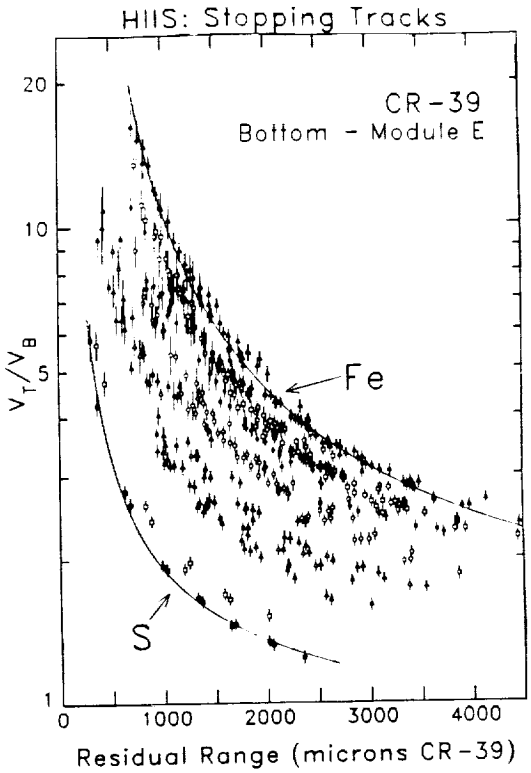


Figure 2: Raw data on stopping tracks found in 10 detector sheets near the bottom of the main stack in Module E. The figure shows data from ~40 cosmic ray tracks, each of which is measured in ~11 detector surfaces on average. The ordinates are the track detector response $V_T/V_B$ and the abscissae are the distance from the stopping end of the track.

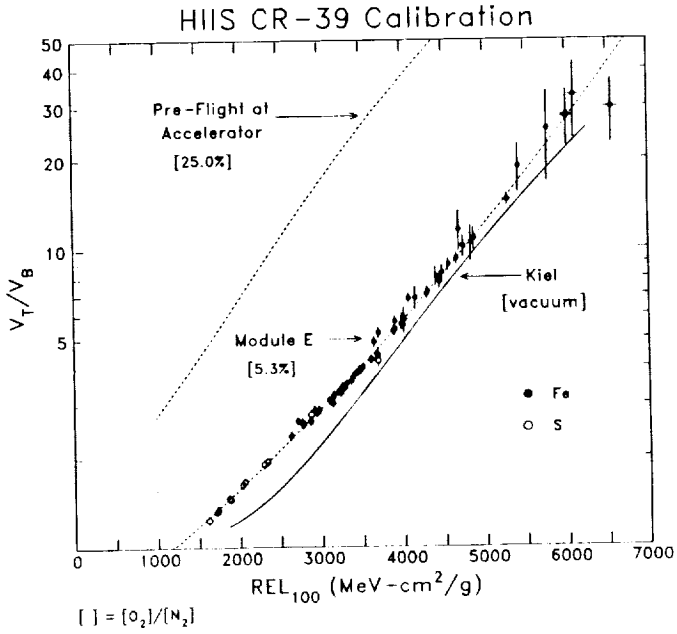


Figure 3: Derived detector response function, as discussed in text. For comparison, also shown are the pre-flight accelerator calibration in air and the Kiel calibration for CR-39 in vacuum[31]. The number in brackets is the measured $O_2/N_2$ ratio in the detector module's gas volume.

## STATUS OF THE STOPPING HEAVY ION ANALYSIS

To date we have used automated scanning to locate 329 stopping tracks in the sheets etched so far, with 70% of the tracks coming from 30 sheets near the top of Module E, under 1.6 g/cm$^2$ of the detector. Each stopping track was then followed and measured through at least 19 detector surfaces or as many as allowed by the etching condition in equation (1) and/or the restricted number of etched sheets. For each track, the set of $V_T/V_B$ vs. residual range measurements was fitted to the response function of Fig. 3, using a Marquardt minimization of $\chi^2$, allowing two free parameters: the atomic number "Z" (which was allowed to take on non-integer values) and "d", the ion's penetration into the stopping sheet (which was typically measured to within an uncertainty of ~ 10 microns)[4*] . Fig. 4 shows a sample of tracks from the

[4*] The mass number A was assigned from a piecewise continuous function of Z, which interpolated between the average A value at each integer Z.

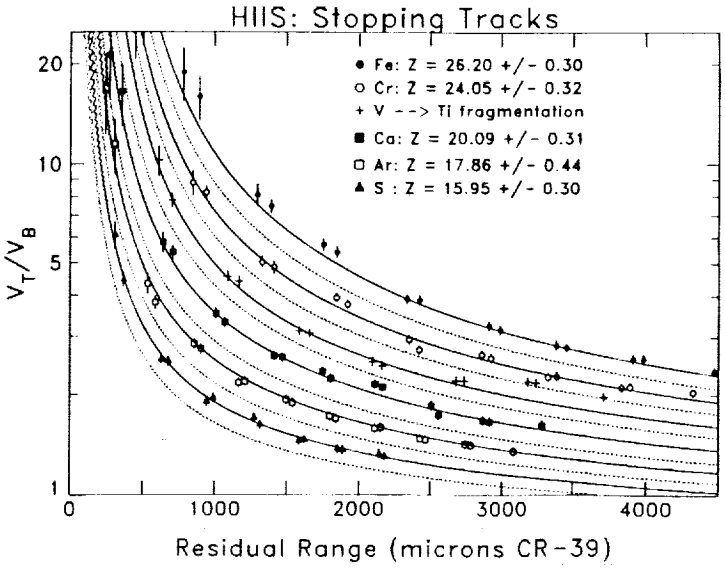


Figure 4: A sample of 6 stopping tracks, each represented with a different symbol. For clarity, only even Z-tracks are shown. The fitted atomic numbers with errors are also shown. Calibration curves, derived from the response function in Fig. 3 are shown for elements 15-26 (solid line: even-Z; dashed line: odd-Z). Note the fragmentation V to Ti.

main stack in Module E, along with the fitted Z values and the formal error calculated by the minimized-$\chi^2$ analysis. In Fig. 5, we show the charge histogram for the 246 successfully-fitted stopping tracks[5*]. To maximize statistics, the figure includes all of the collected stopping tracks, including those which passed through large amounts of shielding by entering through the side or bottom of the detector.

To indicate the quality of the track fits, Fig. 6 shows histograms of the reduced $\chi^2$ and of the errors in the fitted Z value, (as calculated by the minimized-$\chi^2$ analysis) for the successfully fitted tracks. Our track fits give acceptable values of reduced $\chi^2$, and the typical fitted error on Z is ~0.3 charge unit.

Fig. 5 appears to show elemental resolution, with clear peaks centered at integer Z values. We have fitted the charge distribution to a sum of gaussians, leaving the amplitudes, standard deviations, and means as free parameters. This fit, which gives reduced $\chi^2 = 0.6$ for 15 degrees of freedom, is shown in Table 2. Excluding the weak "peaks" at $Z > 26$, $Z < 18$, $Z = 19$, and $Z = 21$, all of the gaussians are centered near integer Z; they have an average $\sigma = 0.30$ charge units. This is good charge resolution for a large space-based plastic-track-detector experiment, comparable to the best results previously achieved[24]. As one would expect, this resolution is consistent with the errors on the individual track fits (Fig. 6b). As shown in Table 2, this resolution is also consistent with Monte Carlo simulations of the detector, which took into account all known factors, including measurement errors, observable track length, the observed non-uniformity in the plastic bulk etch rate, and smearing due to multiple isotopes.

The charge histogram has, however, one surprising feature: the strongest accumulation is at Mn, not Fe. Such a composition is inconsistent with all known sources of cosmic rays, in which the ratio Mn/Fe ~ 0.1 or smaller. This makes it very difficult to believe that the composition shown in Fig. 5 is correct.

[5*] Forty tracks (12% of the total) had too few precise $V_T/V_B$ measurements (because of the restricted number of etched sheets) to be reliably fit; 18 tracks (5%) were identifed as fragmenting in the measured sheets; 25 tracks (8%) failed to give a good $\chi^2$ for unidentifed reasons.

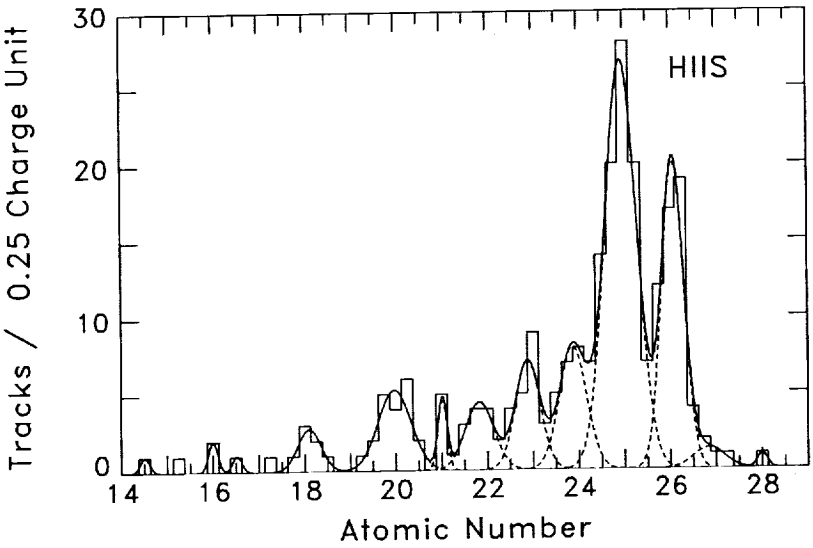


Figure 5: Histogram of fitted atomic numbers of the stopping ions. The histogram was fitted to a sum of gaussians, with results as given in Table 2 below.

TABLE 2 Fit to Sum of Gaussian: Fit Parameters & Their Errors

| | No. Tracks | Mean | Sigma | MC Sigma* |
|---|---|---|---|---|
| S | 2.0 ± 1.4 | 16.00 ± 0.12 | 0.10 ± 0.11 | -- |
| Ar | 7.1 ± 3.6 | 18.10 ± 0.11 | 0.26 ± 0.12 | 0.27 ± 0.01 |
| Ca | 19.1 ± 5.4 | 19.97 ± 0.10 | 0.36 ± 0.07 | 0.29 ± 0.01 |
| Sc | 4.6 ± 2.4 | 21.02 ± 0.08 | 0.10 ± 0.05 | 0.20 ± 0.01 |
| Ti | 13.9 ± 5.1 | 21.83 ± 0.15 | 0.31 ± 0.15 | 0.30 ± 0.01 |
| V | 19.3 ± 6.5 | 22.88 ± 0.11 | 0.27 ± 0.13 | 0.28 ± 0.01 |
| Cr | 23.9 ± 6.7 | 23.87 ± 0.15 | 0.30 ± 0.15 | 0.31 ± 0.01 |
| Mn | 91.8 ± 13.9 | 24.95 ± 0.06 | 0.34 ± 0.07 | 0.35 ± 0.02 |
| Fe | 48.7 ± 9.2 | 26.07 ± 0.06 | 0.24 ± 0.04 | 0.29 ± 0.02 |
| Co | 4.6 ± 3.5 | 26.85 ± 0.52 | 0.34 ± 0.36 | -- |
| Ni | 1.0 ± 1.1 | 28.00 ± 0.17 | 0.11 ± 0.18 | -- |

*Fitted widths of a Monte Carlo simulation of this element in the HIIS detectors.

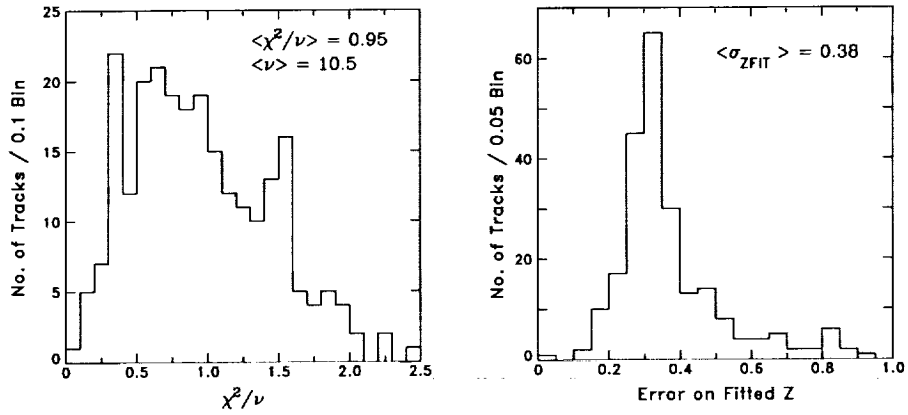


Figure 6: (a) Histogram of the reduced $\chi^2$ values for the tracks in Fig. 5. The average value of reduced $\chi^2$ is 0.95, for an average of 10.5 degrees of freedom. (b) Histogram of the errors on the fitted Z values. The distribution peaks at 0.3, and the average error on the fitted Z is 0.38.

We have made strenuous efforts to understand the "Mn" peak as an error or artifact but have not yet succeeded in doing so. First of all, one cannot simply shift the charge histogram by one unit, since this produces an equally unsatisfactory (Co+Ni)/Fe ratio of ~0.5. Second, the "Mn" peak is obviously not a simple fragmentation effect, since at these energies (> 100 MeV/n), incident Fe would yield fragments uniformly distributed across the sub-Fe elements. Third, the tracks in the "Mn" and "Fe" peaks cannot be separated by selection cuts on quantities like incidence angle, track length, penetration depth into the stopping sheet, $\chi^2$ of the fit, location in the sheets, etc. Finally, the peak structure in Fig. 5 is highly unlikely to be statistical fluctuation: when we force the histogram at $Z > 24$ to fit a single gaussian, we get $\sigma = 0.8$, but with $\chi^2/NDF = 3.2$.

We have also verified that the charge histogram is not an artifact of our analysis software. In particular, our Monte Carlo program yields "simulated data" identical in format to that produced by our microscope data-acquisition programs. We used the Monte Carlo to simulate severely smeared data from a detector with no intrinsic resolution. When we passed these data through an "end-to-end" test of our analysis programs, they produced a flat charge distribution with no statistically significant peaks. The multiple peaks in Fig. 5 are thus a real feature of the data.

At this point, the only detector effects which we have not yet ruled out are (1) a sudden shift in the detector calibration; or (2) a continuous drift in the calibration, with particles collected episodically. In either case, it is further required that the calibration shift correspond almost exactly to $\Delta Z = 1$ unit. Such a calibration shift seems unlikely, but further analysis will enable us to confirm or exclude this possibility. In particular, 85% of the data in Fig. 5 comes from a single module. We have seven other modules, each with a different calibration. Although environmental effects may have conspired to produce a calibration shift of $\Delta Z = 1$ in one module, it is highly unlikely that the shift could be the same in all the modules. When we collect enough tracks from the same depth in a second module, it should be immediately clear whether or not the compositional anomaly shown here is real. Until then, we emphasize that the above results should be regarded as preliminary.

If we take the charge identifications in Fig. 5 at face value, the incident composition of stopping particles apparently varies with energy. When we select the highest energy tracks, with incident energy at the surface of LDEF > 800 MeV/n and which have passed through an average of 33 g/cm$^2$ of aluminum plus plastic, we observe a (Sc-Mn)/Fe ratio of $2.2 \pm 0.6$. This agrees with the value of 2.0 we calculate by propagating an incident galactic cosmic ray composition and spectrum through a mass model of the satellite[22] to the observation point. On the other hand, near the top of the stack, under only 2.6 g/cm$^2$ and at incident energies 140-280 MeV/n, we observe (Sc-Mn)/Fe = $3.2 \pm 0.8$, grossly inconsistent with both galactic and solar energetic particle (SEP) composition.

At low energies, our composition appears to be consistent with previous reports on below-cutoff heavy-ions observed in the magnetosphere. At 140-280 MeV/n, we observe (Sc-Cr)/Fe = $1.3 \pm 0.4$. Previously-reported values are $1.2 \pm 0.3$ (at 25-125 MeV/n; Ref. 3) and $1.5 \pm 0.7$ (at 50-250 MeV/n; Ref. 4). It should be noted, however, that this apparent good agreement may be accidental because (1) the HIIS data may contain Fe from SEP events, whereas the results from Refs. 3 and 4 are not contaminated by SEPs; and (2) it is not clear from their published data that the other experiments have sufficient resolution to separate Mn and Fe. If Fig. 5 were correct, how they handled Mn would greatly affect their value for this ratio.[6*]

---

[6*] If we assume that all of our "Mn" tracks are really Fe, we get a low-energy sub-Fe/Fe ratio of ~0.5. This is consistent with normal galactic cosmic ray composition. But at such low energies, fully-ionized galactic cosmic rays cannot reach the LDEF orbit. As discussed below, partially-ionized solar-energetic particles can penetrate to the LDEF orbit. But in that case, we would expect a sub-Fe/Fe ratio of only a few percent. Thus, even if the "Mn" is spurious, the origin of these low-energy Fe group ions remains unclear.

## STOPPING HEAVY ION FLUXES

*Charge State of Solar Energetic Particles.* Fig. 7 shows our results to date on Fe. In this plot, the fluxes are corrected back to the surface of the satellite, taking into account fragmentation losses. (Feed-down from heavier elements is negligible since the abundance of elements heavier than Fe is only ~5% of Fe.) The GCR curve in Fig. 7 is an absolute prediction, averaged over the solar-cycle variation during the HIIS mission[23] and convoluted with the geomagnetic transmission function. The transmission function was calculated using techniques described in Ref. 24 and averaged over the observed arrival directions, which were primarily from the west, where the cutoff is lowest. The transmission function also took into account cutoff suppression caused by geomagnetic storms. To do this, we used the model of Flueckiger, Shea, and Smart (Ref. 25, hereafter FSS) to calculate suppressed cutoffs for nine different levels of geomagnetic activity, corresponding to $K_p$=0-8$^+$. These nine transmission functions were then combined in a weighted average, with relative weights determined from a survey of the frequency of various $K_p$ conditions during the mission.

At the highest energies, our observed Fe flux is consistent with galactic cosmic rays. Galactic cosmic rays do not, however, account for the observed flux below ~800 MeV/n. We have also argued[26] that the flux at 600 MeV/n is also too large to be due to albedo. These particles may, however, come from the very large SEP events which occurred during the LDEF mission. At ~1 MeV/n, SEP Fe is known to be only partially-ionized[27], with a mean charge of 13.9 $\pm$ 0.5. If this charge state distribution is independent of the energy, SEPs might explain at least part of the observed flux.

To estimate the SEP contribution to the HIIS observations, we obtained from the University of Chicago instrument on IMP-8 a survey[28] of solar flare events during the HIIS mission. Preliminary results from this survey show that only 3 flares (Sept 29, Oct 16, and Oct 24 1989) produced significant Fe flux at

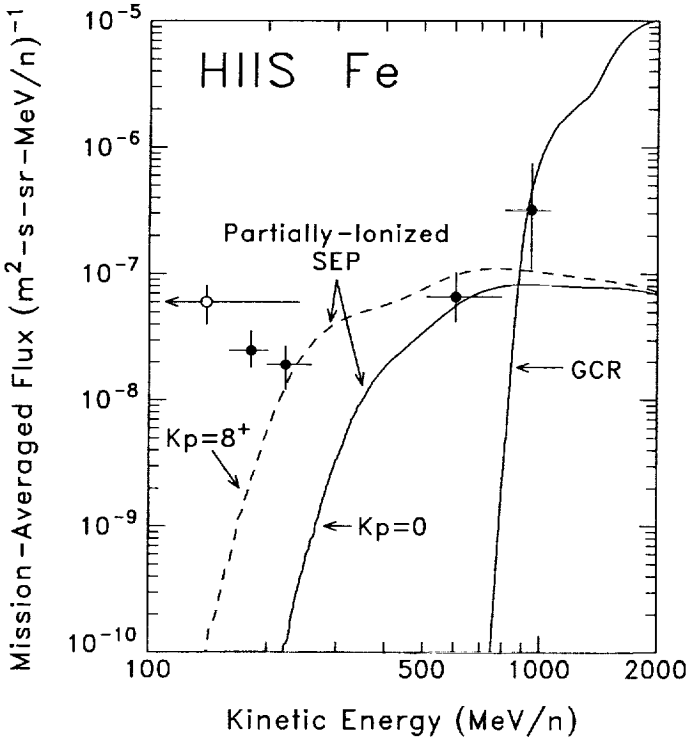


Figure 7: HIIS Fe flux measurements inside the magnetosphere, compared to galactic cosmic rays (GCR) and to partially-ionized SEPs, transmitted through a quiet magnetosphere ($K_p$=0, solid line) and a stormy magnetosphere ($K_p$=8$^+$, dashed line). The open circle at 40-240 MeV/n is a measurement from the Kiel experiment[31] on LDEF of $Z \geq 20$ ions, of which only 30-50% are estimated to be Fe.

200-400 MeV/n. For these three flares, the Chicago instrument provided both fluences and spectral indices. We used these indices to extrapolate to both lower and higher energies. We then transmitted the SEP flux to HIIS, assuming the Fe ions to have the same charge state distribution at all energies as observed at 1 MeV/n. To estimate the effect of geomagnetic storms, we made the calculations twice, once for a quiet magnetosphere ($K_p$=0) and once for a highly-disturbed magnetosphere ($K_p$=$8^+$), using the FSS cutoff suppression model. The results of these calculations are also shown in Fig. 7. At low energies, there is still more flux than this calculation accounts for.[7*] At ~600 MeV/n, however, the HIIS flux agrees well with the extrapolation from the IMP-8 measurements. In fact, assuming all of the observed Fe at 600 MeV/n are solar energetic particles implies an average charge state $\langle Q \rangle = 13.8 \pm 0.9$ (stat) $\pm$ 1.5 (syst), where the statistical error considers only that of the presently available HIIS data and the systematic error is an estimate of the uncertainty in geomagnetic transmission. This preliminary result is in good agreement with the measured mean charge state at 1 MeV/n.

Note that Fig. 7 grossly overstates the range of uncertainty in the SEP flux caused by geomagnetic activity. In particular, our preliminary survey of geomagnetic activity during the HIIS mission shows that a magnetic storm as large as $K_p$=$8^+$ never occurred simultaneously with the arrival of solar energetic Fe ions. With a careful phasing of the observed exomagnetospheric SEP fluxes, geomagnetic activity, and the LDEF orbit, the geomagnetic uncertainty in the SEP charge state determination can be greatly reduced.

We will continue our study of solar energetic ions in the HIIS detectors, in order to measure the charge state of solar energetic Fe and possibly other elements, such as Ca. The measurements in Fig. 7, which fall just below and just above the energy range of IMP-8 measurements, come from sheets at the top and bottom of a module. In between there are 240 unetched sheets per module, which we can use to increase statistics and to trace out the Fe spectrum at the same energies as the IMP-8 measurements. Data on composition and arrival directions will also provide unique signatures of solar energetic particles (namely, sub Fe/Fe ~0.01 after correcting for fragmentation in the detector and arrival overwhelmingly from the directions of lowest cutoff). We will reduce uncertainties in the geomagnetic transmission by carefully phasing the SEP flux, geomagnetic activity, and the LDEF orbit. To test the reliability of our cutoff calculations, we will do ray tracing calculations from points along the LDEF orbit, using the program of Flueckiger et al.[29] and the Tsyganenko model[30] of the magnetosphere.

*Low Energy Ions of Unknown Origin.* Fig. 7 shows a larger Fe flux below 200 MeV/n than even partially-ionized SEPs may be able to account for. (Such a conclusion, however, requires more thorough study of geomagnetic transmission at low rigidities.) As shown in Fig. 7, our observed flux is in good agreement with preliminary results from another LDEF experiment[31]. We also appear to have a strong compositional anomaly at these energies, similar to previous reports[2-5]. At present the origin of these low energy particles is not understood. In future work, we will use the HIIS data to extend observations of these ions, in order to clarify their origin. With the top detector stacks, we can follow the Fe flux down to ~30 MeV/n. This spectral information, combined with our data on composition and arrival directions, may be used to test models for the origin of these particles, such as albedo, quasi-trapping, and a new exomagnetospheric source.

*Anomalous Component.* We plan to use the HIIS data to extend observations of the anomalous component (AC) to ~300 MeV/n. These particles are known to be singly-ionized[32], which greatly increases their transmission through Earth's magnetic field to LDEF's orbit. At energies below ~100 MeV/n neither galactic cosmic rays nor partially-ionized SEPs can penetrate to the LDEF orbit. At ~100-300 MeV/n, galactic cosmic rays are still geomagnetically excluded, and SEPs should be only a small and calculable background[8*]. Fig. 8 shows a simulation of HIIS measurements of anomalous component Ne

---

[7*] If the "Mn" tracks in Fig. 5 are taken as Fe, the low energy fluxes increase by a factor of ~3, making the apparent excess even larger.

[8*] Arrival direction distributions may be useful in separating SEPs and AC particles at these energies: the singly-charged AC ions have high rigidities which give them unimpeded access from all directions. SEPs at these energies, on the other hand, can only reach HIIS from westerly arrival directions, where the cutoff is lowest.

and Ar. In this figure, the flux expectations are derived from a power-law extension of the AC oxygen flux[33] at ~1 AU, averaged over the solar cycle variation[34] during the LDEF mission, and scaled and shifted in intensity and energy according to the factors given in Ref. 35. The open symbols show the statistical precision we can achieve *using only 10% of the detector area*, except for Ar above 85 MeV/n, where the simulated precision would require all of the available area. If the flux falls more steeply than these extrapolations suggest, we will place upper limits on the high energy AC spectrum. In either case, our results will give new information on the capabilities of the AC accelerator, which is believed to be at the solar wind termination shock.

The solid points in Fig. 8 show the 90% CL upper limits we have obtained so far. The Ar upper limit is actually based on 5 observed tracks. We treated these in an upper limit, pending an estimate of possible background from SEPs and their fragments at E > 150 MeV/n. The Ne flux limit at ~75 MeV/n comes from a null result in scanning 1.2% of the available area, using only a portion of a single detector sheet.

By using Lexan UV enhancement, we should also be able to observe anomalous oxygen at energies of 30-50 MeV/n in the top detector stacks, with statistical precision comparable to that of the Ne simulation in Fig. 8. We will also search for evidence of the anomalous component in the spectra of other elements.

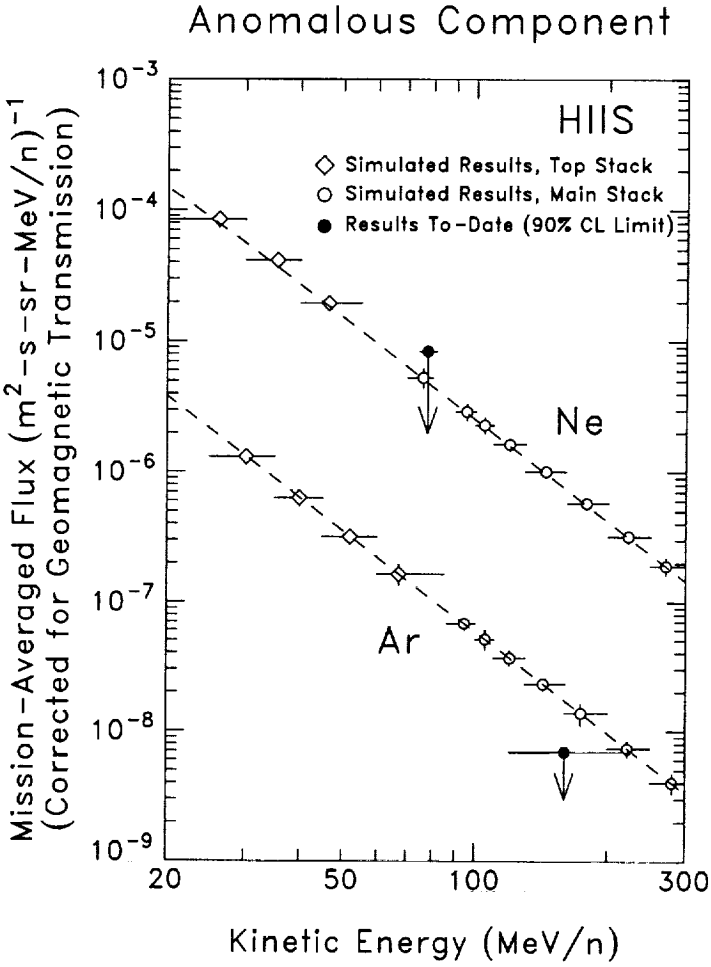


Figure 8: Simulation of HIIS measurements of anomalous component Ne and Ar, assuming they continue as a power law from low energy observations. (Where not visible, the error bars are smaller than the symbols.) Also shown are HIIS upper limits achieved so far. See text for details.

## STATUS OF THE ULTRAHEAVY GALACTIC COSMIC RAY ANALYSIS

In Ref. 18, we outlined our method of analyzing ultraheavy galactic cosmic ray tracks. To date we have collected 127 relativistic ultraheavy cosmic rays with $Z > 45$ by scanning a portion of sheets at the top of Module E. Extrapolating from this result, we expect a total of $1120 \pm 100$ tracks at $Z > 45$ in the seven modules which did not leak. (For comparison, the HEAO dataset[36] contained ~370 nuclei in this charge range.) Based on the time it took to collect and measure the tracks in Module E, we estimate that 3 microscopist-years will be required to obtain the entire ultraheavy dataset.

## CONCLUSIONS

The HIIS data appear to show stopping heavy-ions from a several sources, including galactic cosmic rays and solar energetic particles. Below ~200 MeV/n, there also appears to be an additional source, whose nature is not yet understood. At low energies we also appear to have a strong compositional anomaly, with a large sub-Fe/Fe ratio, apparently consistent with earlier reports[2-5] and preliminary results from another LDEF experiment[31].

In future work, we will extend our observations to a second HIIS module, to confirm or refute our compositional anomaly. We will also collect data from the ~250 unetched sheets in the middle of the stack, so as to search for SEPs in the 200-400 MeV/n energy range covered by the IMP-8/Chicago measurements. We will also make more detailed studies of geomagnetic transmission at low rigidities, using the ray-tracing program of Ref. 29, to fully understand the SEP contribution to our data. Once we have understood the SEP contribution, we should be able to separate out the unknown low-energy component. Using detector sheets nearer to the top of the module, we can follow the Fe-group flux down to ~30 MeV/n. This spectral information, combined with our data on composition and arrival directions, may be used to test models for the origin of these particles, such as albedo, quasi-trapping, or a new exomagnetospheric source.

## ACKNOWLEDGEMENTS

We greatly thank Bill Dietrich for providing us with preliminary IMP-8 data on SEP events during the HIIS mission. We thank Bonnie Colborn for her generous assistance in running the LDEF mass model program. We also thank Rudolf Beaujean for discussions of his observations of stopping heavy ions on LDEF. This work has been supported by the Office of Naval Research and NASA.

## REFERENCES

1. Krause, J.: Magnetische-verbotene Teilchen mittlerer Energie bei der Spacelab 1 Mission, Ph.D. thesis, Institute fuer Kernphysik, Univ. Kiel, FRG, 1986.
2. Biswas, S. et al.: Observation of Low-Energy (30-100 MeV Nucleon$^{-1}$) Partially Ionized Heavy Ions in Galactic Cosmic Rays. Astrophys. J. Letters, vol. 359, 1990, pp. L5-L9.
3. Biswas, S. et al.: Ratio of Sub-Iron (Sc-Cr) To Iron Ions in Low Energy Galactic Cosmic Rays Inside & Outside of Earth's Magnetosphere. Proc. 22nd ICRC (Dublin), vol. 2, 1991, pp. 308-311.
4. Gargarin, Yu.F. et al.: Sulfur-Nickel Nuclei at Small Energies in Cosmic Rays, Proc. 21st ICRC (Adelaide), vol. 3, 1990, pp. 11-14.
5. Grigorov, N.L. et al.: Heavy Ions in Cosmic Rays. Sov. J. Nucl. Phys. (Yadernaya Fizica), vol. 53, 1991, pp. 827-834.
6. Mitra, B. et al.: Implications of the Observations of Partially Ionised States in Low Energy Galactic Cosmic Rays. Proc. 22nd ICRC (Dublin), vol. 2, 1991 pp. 312-315.
7. CR-39 is poly diethylene glycol bis-alyl carbonate and was invented at Pittsburgh Plate Glass's Columbia Resin Laboratory in Barberton, OH.
8. Adams, J.H.Jr.: A Curing Cycle for Detector-Quality CR-39. Nucl. Tracks: Meth., Inst. and Appl., Suppl. 3, 1982, pp. 145-148.

9. Tarle, G.: Improvement of the Etching Properties of CR-39 Plastic Track Detectors. Proc. 17th ICRC (Paris), vol. 8, 1981, pp. 74-77.
10. Lexan is the trade name for bis-phenol A polycarbonate, as sold by General Electric, Pittsfield MA. It is also sold under the tradenames of Tuffak and Rodyne-P.
11. Stiller, B.; Adams, J.H.Jr.; and Beahm, L.P.: Ultraviolet Enhancement of Tracks in Lexan with Black Fluorescent Lamps. Nucl. Tracks, vol. 12, 1986, pp. 137-40.
12. O'Sullivan, D. et al.: The Ultra Heavy Cosmic Ray Experiment. Proc. First LDEF Post-Retrieval Symposium, NASA CP-3134, Part 1, 1991, pp. 367-375.
13. Kapton is a polyamide plastic manufactured by Du Pont Inc., Wilmington, DE.
14. Fleischer, R.L.; Price, P.B.; and Walker, R.M.: *Nuclear Tracks in Solids: Principles and Applications.* (Berkeley: University of California Press), 1975, pp. 57-63.
15. Benton, E.V. and Nix, W.D.: The Restricted Energy Loss Criterion for Registration of Charged Particles in Plastics. Nucl. Inst. Meth., vol. 67, 1969, pp. 343-7.
16. Henke, R.P. and Benton, E.V.: On Geometry of Tracks in Dielectric Nuclear Track Detectors. Nucl. Inst. Meth., vol. 97, 1971, pp. 483-9; Somogyi, G. and Szalay, S.A.:Track-Diameter Kinetics in Dielectric Track Detectors. Nucl. Inst. Meth., vol. 109, 1973, pp. 211-32.
17. Adams, J.H.Jr.: Automated Track Measurements in CR-39. Nucl. Tracks, vol. 4, 1980, pp. 67-76.
18. Adams, J.H.Jr.; Beahm, L.P.; and Tylka, A.J.: Preliminary Results from the Heavy Ions in Space Experiment. Proc. First LDEF Post-Retrieval Symposium, NASA CP-3134, Part 1, 1991, pp. 377-391.
19. Drach, J. et al.: Effect of Oxygen on Response of Plastic and Glass Track Detectors. Nucl. Inst. Meth., vol. B28, 1987, pp. 364-8.
20. Yadav, J.S. and Singh, R.K.: Change of CR-39(DOP) Track Detector Response as a Result of Space Exposure. Nucl. Tracks Radiat. Meas., vol. 17, 1990, pp. 579-82.
21. Adams, J.H. Jr.; Beahm, L.P.; and Tylka, A.J.: The Heavy Ions in Space Experiment: Preliminary Calibration and Analysis. Proc. 22nd ICRC (Dublin), vol. 2, 1991 pp. 523-526.
22. Colborn, B.L. and Armstrong, T.W.: Geometry and Mass Model of Ionizing Radiation Experiments on the LDEF Satellite. SAIC Report No. SAIC-TN-9202, 1992.
23. Nymmik, R.A. et al: A Model of Galactic Cosmic Ray Fluxes. Nucl. Tracks. & Radiat. Meas., vol. 20, 1992, pp. 427-429.
24. Adams, J.H. Jr.; Beahm, L.P.; and Tylka, A.J.: The Charge State of the Anomalous Component: Results from the Trapped Ions in Space Experiment. Astrophys. J., vol. 377, 1991, pp. 292-305.
25. Flueckiger, E.O.; Smart, D.F., and Shea, M.A.: A Procedure for Estimating the Changes in the Cosmic Ray Cutoff Rigidities and Asymptotic Directions at Low and Middle Latitudes During Periods of Enhanced Geomagnetic Activity. J. Geophys. Res., vol. 91, 1986, pp. 7925-7930.
26. Adams, J.H. Jr.; Beahm, L.P.; and Tylka, A.J.: Observations from LDEF of Heavy Ions Below the Geomagnetic Cutoff. Proc. 22nd ICRC (Dublin), vol. 1, 1991 pp. 619-622.
27. Luhn, A. et al.: Ionic Charge States of N, Ne, Mg, Si, and S in Solar Energetic Particle Events. Adv. in Space Res., vol. 4, 1984, pp. 161-164.
28. Dietrich, W.F. 1992, private communication.
29. Flueckiger, E.O. et al.: A New Concept for the Simulation and Visualization of Cosmic Ray Particle Transport in the Earth's Magnetosphere. Proc. 22nd ICRC (Dublin), vol. 3, 1991, pp. 648-651.
30. Tsyganenko, N.A.: A Magnetospheric Magnetic Field Model with a Warped Tail Current Sheet. Planet. Space Sci., vol. 37, 1989, pp. 5-20.
31. Beaujean, R. et al.: in Second LDEF Post-Retrieval Symposium, NASA CP-3194, 1993. private communication.
32. Adams, J.H.Jr. et al.: The Charge State of the Anomalous Component of Cosmic Rays. Astrophys. J. Lett., vol. 375, 1991, pp. L45-L48.
33. Cummings, A.C. and Stone, E.C.: Energy Spectra of Anomalous Cosmic-Ray Oxygen During 1977-1987. Proc. 20th ICRC (Moscow), vol. 3, 1987, pp. 421-424.
34. Mewaldt, R.A.: Temporal Variations of Anomalous Cosmic Rays and Further Evidence for Anomalous Cosmic Ray Hydrogen. Proc. 21st ICRC (Adelaide), vol. 6, 1990, pp. 160-163.
35. Cummings, A.C. and Stone, E.C.: Elemental Composition of the Anomalous Cosmic-Ray Component. Proc. 20th ICRC (Moscow), vol. 3, 1987, pp. 413-416.
36. Binns, W.R. et al.: Abundances of Ultraheavy Elements in the Cosmic Radiation: Results from HEAO 3. Astrophys. J. vol. 346, 1989, pp. 997-1009.